Annu. Rev. Phys. Chem. 1997. 48:213–42

STARK SPECTROSCOPY: Applications in Chemistry, Biology, and Materials Science

Gerold U. Bublitz and Steven G. Boxer
Department of Chemistry, Stanford University, Stanford, California 94305-5080;
e-mail: sboxer@leland.stanford.edu

KEY WORDS: electroabsorption, electrochromism, electro-optic absorption, electric field, charge transfer

ABSTRACT

Stark spectroscopy has been applied to a wide range of molecular systems and materials. A generally useful method for obtaining electronic and vibrational Stark spectra that does not require sophisticated equipment is described. By working with frozen glasses it is possible to study nearly any molecular system, including ions and proteins. Quantitative analysis of the spectra provides information on the change in dipole moment and polarizability associated with a transition. The change in dipole moment reflects the degree of charge separation for a transition, a quantity of interest to a variety of fields. The polarizability change describes the sensitivity of a transition to an electrostatic field such as that found in a protein or an ordered synthetic material. Applications to donor-acceptor polyenes, transition metal complexes (metal-to-ligand and metal-to-metal mixed valence transitions), and nonphotosynthetic biological systems are reviewed.

INTRODUCTION

The effect of an applied electric field on an absorption or emission spectrum is known as the Stark effect. The terms electrochromism, electroabsorption, and electro-optic absorption have also been used in the literature to describe the same phenomenon. This experimental approach has been used to probe the electronic structure of diverse systems, from isolated molecules in the gas phase to the band structure of semiconductors and crystalline materials to complex biological systems. In this review we focus on Stark spectroscopic studies

0066-426X/97/1001-0213$08.00

of molecular transitions in the solid state that employ a lineshape analysis of the Stark spectrum. Most early work focused on accurate measurements of simple molecules primarily as a test of molecular orbital theory; however, these molecules were typically chemically uninteresting. A renaissance of the method has resulted from the simple realization that it can be used for any system as long as a suitable polymer or glassy matrix can be found. Although there are both experimental and conceptual limitations of this approach, a tremendous diversity of molecular systems has been sampled in the past few years, in many cases for the first time.

Two parameters characteristic of an absorption or emission transition are obtained directly: the change in dipole moment, $\Delta\mu$, and the change in polarizability, $\Delta\alpha$, between the initial and final state. $\Delta\mu$ is especially important as the measure of the amount of charge transfer associated with a transition. $\Delta\alpha$ is a measure of the sensitivity of a transition to an applied electric field and is particularly important for understanding the electronic properties of a chromophore interacting with an organized environment such as a protein matrix. Both $\Delta\mu$ and $\Delta\alpha$ can be estimated theoretically but often not very accurately; thus Stark measurements provide information beyond the absorption and emission spectra themselves that can be used to test and extend quantum chemical calculations, especially in the condensed phase.

METHODS

General Comments

The change in transition frequency $\Delta\nu$ of a molecular transition due to an externally applied field $\vec{F}$ is given by $\Delta\nu = -\Delta\vec{\mu} \cdot \vec{F} - 1/2\vec{F} \cdot \underline{\Delta\alpha} \cdot \vec{F}$. The two terms are also known as the linear and quadratic Stark effect, respectively, because $\Delta\mu$ will lead to a frequency shift linear in $|\vec{F}|$ and $\Delta\alpha$ to a shift quadratic in $|\vec{F}|$ for a transition in an uniaxially oriented system. Such uniaxial orientation, though highly desirable, is rarely achieved in practice except in simple systems. Extensive work has been carried out studying the Stark effect on narrow absorption lines characteristic of guest molecules in a host crystal at cryogenic temperatures (1, 2) or on spectral holes burned into the molecule's inhomogeneously broadened absorption band either in crystalline or noncrystalline matrices (3–7). Either approach is very desirable when a suitable host and molecular system are being studied, but appropriate crystal host matrices are often not available for chemically interesting molecules, and the combination of hole burning and Stark spectroscopy requires specialized equipment and a system in which holes can be readily burned. In the following we focus on nonoriented, immobilized molecules, meaning simply that the molecule of interest is dissolved in a solid polymer or frozen glass matrix. The inhomogeneity

of the bands being analyzed limits, to some extent, the information that can be obtained with high accuracy, as discussed in the section below on limitations; however, the technique greatly increases the diversity of molecular systems that can be studied, including ionic compounds that cannot be studied in fluid solution.

Analytical Methods

For an isolated absorption band in a nonoriented, immobilized sample (solid solution) where $\Delta\bar{\nu}$ (the shift of the transition energy upon application of an electric field, usually expressed in units of cm^{-1}) is smaller than the inhomogeneous bandwidth, the change in absorption upon application of an external field is given by (8, 9)

$$\Delta A(\bar{\nu}) = F^2 \left\{ A_\chi A(\bar{\nu}) + \frac{B_\chi}{15hc}\bar{\nu}\frac{d}{d\bar{\nu}}\left(\frac{A(\bar{\nu})}{\bar{\nu}}\right) + \frac{C_\chi}{30h^2c^2}\bar{\nu}\frac{d^2}{d\bar{\nu}^2}\left(\frac{A(\bar{\nu})}{\bar{\nu}}\right)\right\}, \quad 1.$$

with

$$A_\chi = \frac{1}{30|\vec{m}|^2}\sum_{ij}\left[10A_{ij}^2 + (3\cos^2\chi - 1)\left(3A_{ii}A_{jj} + A_{ij}^2\right)\right] + \frac{1}{15|\vec{m}|^2}\sum_{ij}\left[10m_i B_{ijj} + (3\cos^2\chi - 1)(4m_i B_{ijj})\right], \quad 2.$$

$$B_\chi = \frac{5}{2}\mathrm{Tr}(\underline{\Delta\alpha}) + (3\cos^2\chi - 1)\left(\frac{3}{2}\underline{\Delta\alpha}_m - \frac{1}{2}Tr(\underline{\Delta\alpha})\right) + \frac{1}{|\vec{m}|^2}\sum_{ij}\left[10m_i A_{ij}\Delta\mu_j + (3\cos^2\chi - 1) \times (3m_i A_{jj}\Delta\mu_i + m_i A_{ij}\Delta\mu_j)\right], \quad 3.$$

and

$$C_\chi = |\Delta\mu|^2 \cdot \left[5 + (3\cos^2\chi - 1)(3\cos^2\zeta_A - 1)\right], \quad 4.$$

where $\underline{\mathrm{A}}$ and $\underline{\underline{\mathrm{B}}}$ are the transition polarizability and transition hyperpolarizability, respectively, reflecting the influence of the electric field on the transition moment $\vec{m}$: $\vec{m}(\vec{F}) = \vec{m} + \underline{A}\cdot\vec{F} + \vec{F}\cdot\underline{\underline{B}}\cdot\vec{F}$. χ is the experimental angle between the externally applied field and the polarization of the incident light, ζ_A is the angle between $\Delta\vec{\mu}$ and $\vec{m}$, and $\underline{\Delta\alpha}_m$ is the component of the polarizability change along the direction of the transition moment (i.e. $\underline{\Delta\alpha}_m = (\vec{m}\underline{\Delta\alpha}\vec{m})/|\vec{m}|^2$). The

indices *i* and *j* are used for individual components of the vectors and tensors and run over the molecular coordinates *x*, *y*, and *z*.

In the simplest physical terms, the random orientations of $\Delta\vec{\mu}$ relative to the applied field direction lead to a spread in the transition energy; the difference between this broadened lineshape and the lineshape in the absence of a field is just the second derivative of the absorption. The molecular polarizability change, $\Delta\alpha$, interacts with the field to induce a dipole moment typically in the direction of the field. Because this field-induced dipole moment is oriented with respect to the field, the spectrum shifts either to higher or to lower energy, depending on the sign of $\Delta\alpha$; this lineshape is the first derivative of the absorption spectrum. The origin of these observed lineshapes can be understood by looking at a hypothetical sample consisting of only two populations—aligned parallel and antiparallel with respect to the external field, as shown in Figure 1.

Additional terms that depend on $(kT)^{-1}$ and describe the reorientation of the molecules in the applied field have to be considered in Equations 2–4 if the sample is not immobilized (i.e. for liquid solutions) (8, 9). In these cases the second derivative coefficient (C_χ) is usually very small compared with the first (B_χ) and zeroth (A_χ) derivative coefficients. An advantage of the measurements in liquid solution is the simultaneous determination of both the ground state and excited state dipole moments of the studied species. However, information on polarizabilities usually cannot be obtained because of the dominance of the reorientation effect. Experiments in liquid solutions are also limited to uncharged molecules, since in their presence dielectric breakdown occurs at low fields. Previous reviews (8–11) have focused mostly on this experimental approach; thus we emphasize the application of the technique to immobilized samples, especially since in recent years it has been more commonly used.

Decomposition of the ΔA spectrum for an isotropic immobilized sample into absorption derivative components yields values for A_χ, B_χ, and C_χ, which then can be used to extract information on the molecular parameters. The main characteristics of the Stark spectrum can often be obtained from a visual comparison of the lineshapes of the Stark spectrum and the dominant derivative term of the absorption. The derivatives needed for the quantitative analysis can be obtained in two different ways. Direct numerical differentiation of the absorption spectrum requires smoothing of the data prior to taking the derivative in order to decrease the noise level of the derivative. Approximating the data with a third-order polynomial using a sliding window averaging algorithm (Savizky-Golay filter) usually gives the best results. Care has to be taken to maintain the lineshape of the spectrum, both in its curvature and peak intensities. Alternatively, the absorption spectra can be fit to a sum of Gaussian bands whose analytical derivatives are then used to model the ΔA spectrum. Both approaches usually produce identical results. The latter approach can also be

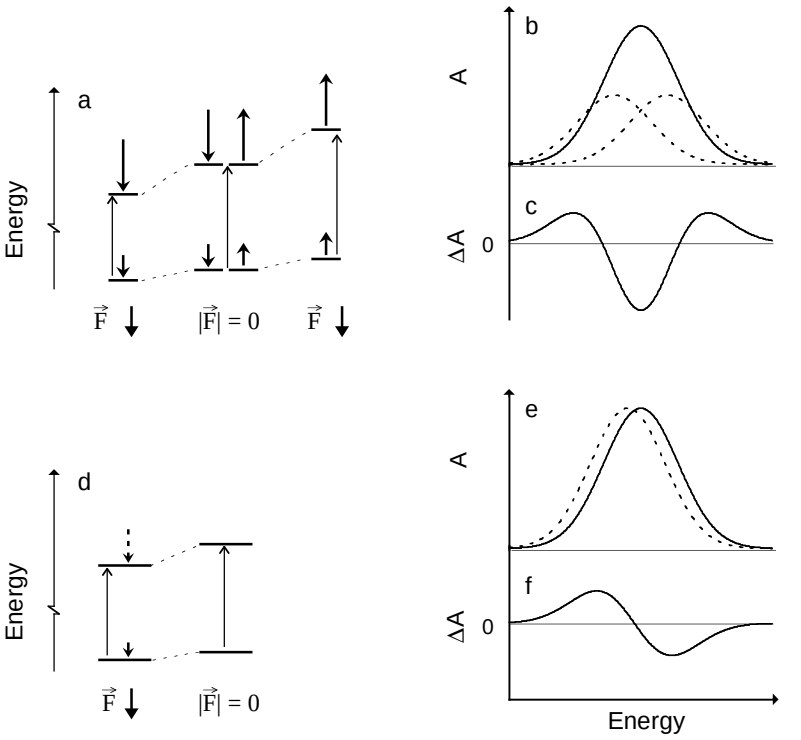

Figure 1 Schematic illustration of the effect of an applied electric field on an absorption lineshape. (*a*) The interaction of an applied electric field with two orientational subpopulations in which $\Delta\mu$ (shown here for $\Delta\mu > 0$) is aligned with or against the field. (*b*) A corresponding inhomogeneously broadened absorption spectrum without (—) and with (- - -) the applied external field. In an electric field the absorption of the two orientational subpopulations shifts to lower and higher energy, respectively, i.e. the band broadens. (*c*) The difference or Stark spectrum (field-on minus field-off) has a second derivative lineshape. (*d*) Interaction of an applied electric field with a transition that has a difference in polarizability, $\Delta\alpha$, between the ground and excited state (shown here for $\Delta\alpha > 0$). (*e*) A corresponding inhomogeneously broadened absorption spectrum without (—) and with (- - -) the applied external field. The applied electric field induces a dipole moment in only one direction, regardless of the molecule's orientation, and the absorption shifts towards lower energy. (*f*) The difference or Stark spectrum (field-on minus field-off) has a positive first derivative lineshape. If $\Delta\alpha < 0$, the absorption energy will shift toward higher energy, and the Stark spectrum will have a negative first derivative lineshape. A change in transition intensity due to an applied electric field will lead to a Stark spectrum with a lineshape similar to the one of the absorption spectrum (zeroth derivative lineshape, not shown). All of these effects may occur simultaneously. The contributions of each effect are obtained by decomposing the Stark spectrum into derivatives of the absorption spectrum.

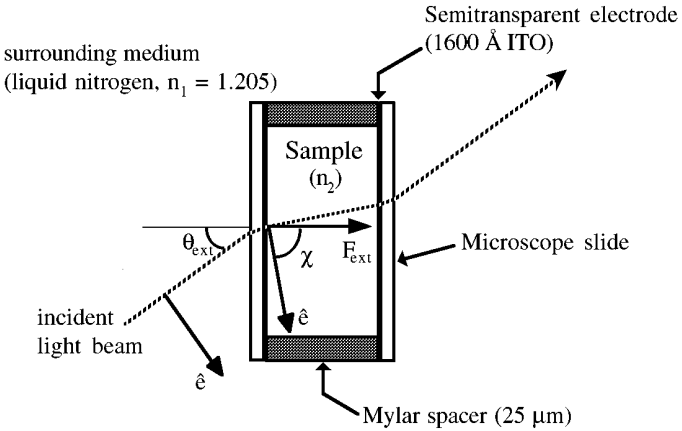

Figure 2 Schematic diagram of a typical sample cell used for measuring Stark spectra in frozen glasses. The semitransparent electrodes coated onto the inner side of the windows are connected to a high-voltage power supply. The experimental angle χ between the externally applied field and the polarization of the incident light beam can be calculated from the external angle θ_{ext} and the refractive indices of the surrounding medium (n_1) and the sample (n_2), using Snell's law: $n_1 \cdot \sin(\theta_{\text{ext}}) = n_2 \cdot \sin(90^\circ - \chi)$.

used as a deconvolution technique for cases where multiple absorption bands with different electro-optic parameters (and thus different values of A_χ, B_χ, C_χ) are present.

The angle ζ_A between the direction of the transition moment $\vec{m}$ and the direction of the difference dipole $\Delta\vec{\mu}$ can be obtained from the second derivative components of Stark spectra taken at different values of χ, which is the experimental angle between $\vec{F}$ and the electric vector of the horizontally polarized light (Equation 4). In cases where the second derivative component dominates the Stark spectrum, ζ_A can be obtained directly from the experimental data after correcting χ using Snell's law and adjusting ΔA for the increased path length as χ increases (cf Figure 2). The value of ζ_A is useful because it describes the direction of charge separation in the molecular axis system associated with a transition (assuming the direction of $\vec{m}$ is known).

Recently the conventional method has been extended to include the higher harmonic responses of the absorption to the applied ac field, a technique called higher-order Stark spectroscopy (HOSS) (12). The field-induced change in absorbance by an externally applied sinusoidal electric field $F(\omega) = F_0 \sin(\omega t)$ is given by

$$\Delta A(\nu, F) = \Delta A(\nu, F^2, 2\omega) + \Delta A(\nu, F^4, 4\omega) + \Delta A(\nu, F^6, 6\omega) + \cdots.$$

The individual terms of this series can be recorded using lock-in detection at the second, fourth, sixth, etc harmonic of the field modulation frequency ω, with the nth-order spectrum depending on the nth power of the applied field F^n. An expression similar to the one given above for the conventional (second-order) Stark spectrum can be obtained for each nth-order spectrum, with the ΔA signal equivalent to a sum of zeroth through nth derivative terms. In every case the nth derivative term depends only upon $\Delta\mu$ and ζ_A. Additionally, it follows that if $\Delta\mu$ dominates the Stark spectrum the $(n + 2)$th-order Stark spectrum is proportional to the second derivative of the nth-order spectrum. This diagnostic tool proves to be very powerful because Stark spectra (and thus their derivatives) can be obtained with good signal-to-noise ratios while higher derivatives of the absorption spectrum are difficult to obtain.

Finally, we mention an interesting variation on Stark spectroscopy that is coupled to the effects of electric fields on chemical reactions, for example electron or proton transfer reactions (13). The rate of a chemical reaction involving charge movement in an electric field should depend on the orientation of the change in dipole moment associated with this charge movement relative to the field direction. For example in the case of electron transfer starting with neutrals and giving a charge-separated state, the free energy change for the reaction will increase or decrease depending on whether the charge-separated state is aligned with or against the field, respectively. Because the rate of the reaction depends on the change in free energy, it should also depend on the orientation in the field. Such orientation-dependent kinetics leads to a transient anisotropic orientational subpopulation of chromophores. The Stark spectrum of this anisotropic subpopulation is no longer described by Equation 1, which is appropriate for an isotropic distribution, but now depends explicitly on the mechanism that led to the anisotropic subpopulation in the field. This effect has been called dynamic Stark effect and was first applied to the analysis of the anomalous lineshape observed for fluorescence from the special pair in photosynthetic reaction centers (this fluorescence occurs in competition with field-sensitive excited state electron transfer) (14). It was later generalized and used to probe complex electron transfer dynamics in reaction centers (15). By comparing the Stark lineshape for an isotropic sample with that when field-dependent processes compete, information on the direction of the dipole moments formed (or consumed) relative to the molecular axes can be extracted.

Experimental Methods

Light from an appropriate conventional source [i.e. a tungsten-halogen lamp for visible (Vis) and near-infrared (NIR) light, a high pressure Xe-arc lamp for near ultraviolet (UV) light] is dispersed through a monochromator, horizontally polarized, and focused through the sample. Si-photodiodes are excellent low

noise detectors from about 400 to 1100 nm and, if they do not have a protective glass coating, can also be used down to about 200 nm. Alternatively, in the near UV a photomultiplier with reduced gain (achieved by wiring only a few dynodes) offers a reasonable compromise between the signal-to-noise ratio and sensitivity. Very few experiments have been carried out in the infrared region that use a combination of a tungsten halogen lamp and a Ge-photodiode detector for the 1–2 μm region (16, 17) and a Nernst glower as excitation source beyond 2 μm in combination with a InSb detector (2–4 μm) or a HgCdTe detector (mid-IR) (18). It should be straightforward to adapt a step-scan Fourier transform IR spectrometer for performing vibrational Stark spectroscopy.

A schematic diagram of a typical sample cell is shown in Figure 2. The sample cell consists of two glass, quartz, sapphire, or silicon slides, coated with a semi-transparent electrode material held apart by a spacer of typically 25-μm thickness. The electrode material depends on the application: Usually indium tin oxide (ITO) is an ideal choice, except for wavelengths below 350 nm. Otherwise Ni, typically 70 Å thick and prepared by evaporation, is about 50% transparent over a wide spectral range. Both ITO and Ni can be overcoated with a thin film of SiO_2 if electrode corrosion is a problem. The compound to be studied has to dissolve in a solvent that forms a good optical quality glass upon freezing, such as a 50:50 (by volume) glycerol:water mixture for aqueous samples (e.g. proteins or ionic compounds) or an appropriate organic solvent (e.g. ethanol, 2-methyltetrahydrofuran, toluene or 3-methylpentane). Alternatively, polymer film samples can be prepared by spin coating an electrode-coated window with a polymer solution containing the sample followed by evaporation of the second electrode onto the dried polymer surface. A free-standing polymer film can be prepared by evaporating the solvent from the polymer solution; the electrodes are then deposited on both sides of the film by standard vacuum deposition techniques, or the film is sandwiched between two electrode-coated windows. Ideally the sample should have a peak absorption of about 0.2–0.6, so fairly concentrated solutions are needed, but Stark spectra can be recorded for samples with much lower optical density. In these cases the accurate detection of the absorption spectrum lineshape that is needed for the analysis of the Stark spectrum can become the limiting factor.

An ac electric field is applied to the sample by a custom-built high-voltage power supply that amplifies a digitally generated sinusoidal voltage (schematics available upon request from SGB). The power supply is equipped with a current fuse that cuts off the applied field upon sensing a current flow and in this way helps to preserve the sample from dielectric breakdown. For frozen organic or aqueous glass samples of 25-μm thickness, electric fields of approximately 1 $MV \cdot cm^{-1}$ can routinely be obtained (modulation frequency typically hundreds of Hertz). The angle χ between the applied field direction and electric

vector of the polarized light (horizontal) can be varied by rotating the sample about the vertical axis. For electronic Stark spectroscopy in the UV, visible, and NIR regions, the samples are immersed in liquid nitrogen in a dewar fitted with strain-free quartz windows. Bubbling of the liquid N_2 is minimized by blowing a thin stream of He gas over its surface. Alternatively, a pumped He dewar can be used if very low temperatures are desired or the sample can be mounted in a miniature Joule-Thompson refrigerator (MMR Technologies) where the temperature can be varied between room temperature and about 80 K.

The signal from the detector is recorded with a lock-in amplifier (Stanford Research Systems) detecting at the second (fourth, sixth, etc for HOSS) harmonic of the applied external field frequency. If the monochromator scan speed and lock-in time constant are chosen carefully, data acquisition can take place in a continuous scan over the wavelength region of interest, leading to a resolution of the Stark data equal to that of the absorption spectrum. The direct output of the detector is recorded as well, since it is needed for the calculation of the change in absorption. If the change in absorption due to the applied external field is small, ΔA can be obtained as

$$\Delta A(\nu, F^2, 2\omega) \cong \frac{2\sqrt{2}}{\ln 10} \frac{\Delta I(\nu, F^2, 2\omega)}{I},$$

and

$$\Delta A(\nu, F^4, 4\omega) \cong \frac{8\sqrt{2}}{\ln 10} \frac{\Delta I(\nu, F^4, 4\omega)}{I}.$$

.

LIMITATIONS

Experimental Limitations

The main experimental limitations are the uncertainties in determining the absorption lineshape and the magnitude of the electric field. The problems in measuring the absorption lineshape are usually systematic in character, since the experiment is essentially a single-beam setup. This can be overcome in part by taking absorption spectra of thicker (and thus optically denser) samples in a cuvette that does not have interfering electrode coatings using a commercial dual-beam spectrophotometer. In this way the absorption lineshape can be recorded, and only its magnitude has to be determined for the actual Stark sample, which for samples immersed in liquid N_2 usually has an error of about ± 0.01 absorbance units. Because the analysis of the Stark spectrum involves derivatives of the absorption, both a good signal-to-noise ratio and accuracy in the wings of the absorption lineshape are required.

The magnitude of the external electric field depends on the sample thickness and the applied voltage. The latter is known accurately, and the former can be determined either mechanically with precision calipers or by observation of interference fringes of the empty sample cuvette. Both of these measurements are done at room temperature, and the values may change upon freezing. Errors due to these sources are estimated to be typically on the order of ± 1–2 μm. Additionally, there is uncertainty in the exact magnitude of the electric field strength felt by the molecule because there is a difference between the externally applied field and the internal field at the position of the chromophore. The internal-field $\vec{F}$ whose magnitude enters into the calculations of the molecular parameters can be expressed as $\vec{F} = \underline{f} \cdot \vec{F}_{\text{ext}}$, where $\underline{f}$ is a tensor describing the local field correction and $\vec{F}_{\text{ext}}$ is the externally applied field. The local field correction $\underline{f}$ can be modeled in different ways, usually as a scalar and depending on the dielectric constant ε of the solvent. One of the simpler approaches uses the model of a spherical cavity created in the solvent by the solute molecule and predicts that $\underline{f} = (\varepsilon + 2)/3$. Modifications in the shape of the cavity (e.g. elliptical) and inclusion of the dielectric constant of the solute molecule lead to more elaborate models (19). To date, no good method has been developed to experimentally determine the local field correction, and this remains a basic limitation when comparing the absolute values of electro-optic parameters obtained by Stark spectroscopy (and many other spectroscopic techniques) with calculated values. It is generally believed that the value of $\underline{f}$ is close to 1.0 and for most frozen organic or aqueous glasses should be on the order of 1.1–1.3. In proteins the value of $\underline{f}$ depends less on the bulk solvent and mostly on the protein matrix around the chromophore of interest. For the case of the photosynthetic reaction center it was concluded that $\underline{f} < 1.3$ based on a comparison of expected and observed electric field effects on the relative energy of a charge-separated state (20). Because one is typically interested in making comparisons among a series of related compounds in the same solvent, the local field correction factor can often be considered a constant factor for the series. For this reason we usually report values of $\Delta\mu$ in units of Debye/$\underline{f}$ and those of $\Delta\alpha$ in units of $\text{Å}^3/\underline{f}^2$, in order to separate uncertainties in the measurement from uncertainties in value of the local field correction factor.

Analytical Limitations

Analytical limitations mainly arise from two origins: the difficulty in obtaining accurate derivatives of the absorption spectra and issues concerning the extraction of molecular parameters from the derivative components (A_χ, B_χ, C_χ). Because the conventional (2ω) Stark signal is usually dominated by the first and second derivative of the absorption spectrum, it is largest in the regions of the

absorption spectrum with high curvature, which is around the peak and wings of the spectrum. Both techniques discussed above for obtaining derivatives—smoothing followed by taking numerical derivatives and fitting the absorption data with Gaussians and using analytical derivatives—are least accurate in the wings of the absorption spectrum. The best approach we have developed to date is to simultaneously fit the absorption and Stark data (21).

The evaluation of $\Delta\mu$ from the second derivative component C_χ (Equation 4) is usually straightforward because there are no other contributions to this component. However, it can be seen from Equation 4 that only information on the magnitude of the difference dipole can be obtained and not on its sign. Complications arise if the inhomogeneously broadened absorption band conceals multiple transitions with different values of the electro-optic parameters (and thus different values of A_χ, B_χ, C_χ). This can arise from different overlapping electronic transitions or the vibronic sidebands that accompany most electronic transitions (22). In these cases the absorption and Stark spectra should be fit to one set of derivative components for each underlying transition. This poses serious problems because the lineshapes of the different absorption bands need to be known accurately. If no separation of the different features can be observed, the single derivative-parameter set will be a suitably weighted average for the underlying bands. In those cases where at least some separation can be observed, e.g. vibronic structure in low-temperature spectra, meaningful information can be obtained for the separate transitions provided that care is taken not to produce artificial values due to interfering effects on the two bands (ΔA for each can be either positive or negative). One band usually dominates the Stark effect, and one way to deal with this problem is to fit the whole band first to one set of derivative parameters, leading to electro-optic parameters (i.e. $\Delta\mu$ and $\Delta\alpha$) that mostly reflect this dominant transition. This is followed by another round of fitting, now using two derivative parameter sets, but with the set representing the dominant transition fixed to the previously obtained values. Although the values obtained this way will not correspond exactly to those of the individual bands, trends in their differences can be determined reliably. The advantage of working in crystalline matrices with very sharp transitions or using hole burning is that these problems can be minimized. Unfortunately, most samples cannot be studied easily this way.

The first derivative component B_χ (Equation 3) has contributions from two different origins, the difference in polarizability between the involved states ($\Delta\alpha$) and cross terms of $\Delta\mu$ and the transition polarizability $\underline{A}$. These latter contributions are often neglected, and values of $\Delta\alpha$ are extracted directly from B_χ. For moderately large values of $\Delta\mu$, however, even rather small values of $\underline{A}$ will lead to a considerable first derivative contribution of the cross terms, leading

to a significant source of uncertainty in $\Delta\alpha$. For intense optical absorptions such as those usually studied in Stark experiments, $\underline{A}$ is expected to be very small[1]; thus the direct calculation of $\Delta\alpha$ from B_χ may be justified in many cases. Contributions from the two components $\underline{A}$ and $\underline{\underline{B}}$ to the zeroth derivative component A_χ (Equation 2) cannot be separated based on the experimental results alone. However, since the contributions from $\underline{A}$ will be positive, $\underline{\underline{B}}$ will be nonnegligible in those (commonly found) cases where the zeroth derivative component is found to be negative.

Conceptual Limitations

A fundamental assumption underlying the application of Equation 1 is that the electro-optic parameters (i.e. $\Delta\mu$ and $\Delta\alpha$) are constant across the absorption band. While this assumption seems to be reasonable for $\Delta\alpha$, it does not necessarily hold for $\Delta\mu$. The total dipole moment μ for a molecule in a given solvent environment consists of two parts: its intrinsic dipole moment μ_0 and the dipole moment induced by its environment μ_{ind}, $\vec{\mu} = \vec{\mu}_0 + \vec{\mu}_{\text{ind}}$. The effect of the environment (i.e. the solvent) on the solute can be viewed as that of a microscopically present strong matrix electric field $\vec{F}_{\text{int}}$ inside the solution and $\vec{\mu}_{\text{ind}} = \underline{\alpha} \cdot \vec{F}_{\text{int}}$. Note that this matrix electric field should not be confused with the local field correction factor. Accordingly, a large value of $\Delta\alpha$ in the presence of a distribution of matrix electric fields will lead to a large distribution in $\Delta\mu_{\text{ind}}$, which might make it impossible to fit the Stark spectrum to a sum of derivatives of the absorption spectrum, especially for molecules with an intrinsically small $\Delta\mu$ but a large $\Delta\alpha$. Thus the interactions that give rise to inhomogeneous broadening can also lead to a distribution of measured values of $\Delta\mu$; this phenomenon has been studied extensively by hole burning Stark spectroscopy (23–27). Vauthey et al (26) found that $\Delta\mu_{\text{ind}}$ varied by about 50% across the inhomogeneously broadened absorption band of a centrosymmetric squaraine dye embedded in a polyvinylbutyral polymer matrix. We measured the conventional Stark spectrum of this system and, as expected, could not fit it to a sum-of-derivatives expression (27a). Furthermore, as mentioned above, the intrinsic difference dipole moment ($\Delta\mu_0$) is expected to change across

[1]This can easily be seen from an expression for $\underline{A}$ derived using perturbation theory: For the transition between the ground state (S_0) and first excited state (S_1), $A \propto \sum_i e^2 \langle S_1|\mathbf{r}|i\rangle\langle i|\mathbf{r}|S_0\rangle$. This expression for $\underline{A}$ involves the interaction of both the ground state S_0 and the excited state S_1 with one virtual state i. For a strongly allowed transition S_1 will be of ungerade symmetry. Since S_0 is of gerade symmetry, the term for $\underline{A}$ will be symmetry forbidden. A similar expresson for $\underline{\underline{B}}$, $B \propto \sum_i \sum_j e^3 \langle S_1|\mathbf{r}|j\rangle\langle j|\mathbf{r}|i\rangle\langle i|\mathbf{r}|S_0\rangle$, involves two virtual states i and j. For i having ungerade symmetry and j gerade symmetry, this term will be symmetry allowed, explaining the commonly observed dominance of $\underline{\underline{B}}$ in the zeroth derivative component.

an inhomogeneously broadened absorption band if it conceals multiple transitions with different intrinsic values of $\Delta\mu_0$. In such a case the observed Stark spectrum might also deviate from a pure sum-of-derivatives lineshape, as was predicted for another case in which coupling of two transitions can lead to changed lineshapes (vide infra) (28).

Finally, there is the possibility that the basic formalism underlying Equation 1 is inappropriate for a particular molecular system. Electric-field–induced mixing of states can lead to new transitions to formerly forbidden states. This might occur within a molecule or new transitions might arise from the interaction of more than one molecule, a process that is especially likely if the chromophore density is high (e.g. in crystalline systems). The exclusive connection of a second derivative lineshape with a difference in dipole moment between ground and excited state has also been challenged for transitions leading to a doubly degenerate excited state (29, 30), as well as for cases where close-lying dark states might be activated by the electric field (31). To date, though, there is no direct evidence that a breakdown of the basic assumptions leading to Equation 1 plays a significant role in the interpretation of Stark spectra of isolated molecules.

APPLICATIONS

In the following we have selected a few applications of Stark spectroscopy to a diverse set of systems. Two reviews have been published recently that focus primarily on photosynthetic systems (the photosynthetic reaction center, antenna complexes, carotenoids in photosynthetic proteins and electric field effects on electron transfer reactions) (13, 32), so most of our discussion involves applications to other systems. We report molecular parameters derived from the analysis of the Stark spectra in terms of $\underline{f}$, the value of the local field correction. Thus the reported values are independent of the differences in models used to approximate this correction. If the compound's molecular geometry used in this model is not spherical, the individual matrix elements of $\underline{f}$ will not be the same, and the appropriate component of the tensor $\underline{f}$ should be used.

Donor/Acceptor-Substituted Polyenes

Liptay and coworkers have shown that centrosymmetric polyenes in fluid solution exhibit significant excited state dipole moments (33). This counterintuitive observation has been interpreted as a symmetry-breaking effect of the solvent environment. By substituting the ends of a polyene with electron donor and acceptor end groups, a permanent dipole moment is introduced into the molecule, and as a result a large change in dipole moment upon excitation is expected.

The systematic effects of these donor and acceptor groups on the structure of the connecting polyene bridge can be understood with a simple model:

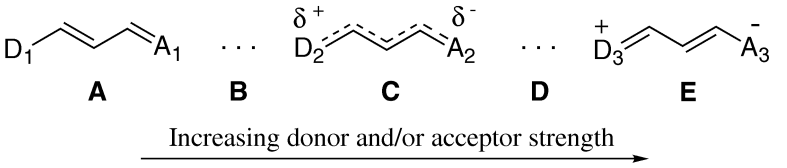

With increasing donor and/or acceptor strength, the bridge will change from a polyene-like structure (limit **A**) toward a more delocalized structure. For fairly strong donor and acceptor end groups, the double bonds in the bridge will be mostly delocalized (limit **C**, the cyanine limit). Upon further increase of donor and/or acceptor strength, the bridge structure will change toward the limit of a charge-separated structure where the double bonds are again localized (limit **E**).

Figure 3 shows the effect of an increase in electron acceptor strength on the electronic structure in a donor/acceptor polyene probed by Stark spectroscopy. Compound **1** has moderately strong donor and acceptor end groups, and the Stark spectrum (panel *b*) is dominated by a second derivative lineshape. The analytical $\bar{\nu}$-weighted second derivative of the compound's absorption spectrum is shown for comparison in panel *c*. The relative magnitude of the positive features in the Stark spectrum deviates from those found in the second derivative spectrum and reveals considerable first derivative contributions. The best fit of the absorption and Stark spectra yields values of $\underline{f} \cdot |\Delta\mu| = 10$ D and $\underline{f}^2 \cdot \Delta\alpha = +1000$ Å^3 (neglecting contributions of A·$\Delta\mu$ cross terms to the first derivative component). This result compares well with expected values for a moderately perturbed polyene bridge structure and assigns **1** to a place close to limit **B**. Compound **2** has the same donor group and chain length as **1** but a stronger acceptor end group. The Stark effect (panel *e*) is much weaker, and the spectrum now has only a small second derivative contribution and is dominated by a negative first derivative lineshape (cf panel *f*). The best fit yields $\underline{f} \cdot |\Delta\mu| = 2$ D and $\underline{f}^2 \cdot \Delta\alpha = -300$ Å^3 (cross term contributions are expected to be very small in this case), a result that is in good agreement with theoretical predictions for cyanine-like molecules and thus places **2** close to limit **C** (34). This example nicely illustrates the power of Stark spectroscopy, even at a qualitative level, for analyzing electronic structure.

The influence of the chain length of the connecting bridge on both ground and excited state dipole moments has been studied in different donor/acceptor polyene systems (34–37). While the ground state dipole moments were found to be only weakly affected by elongating the bridge, the excited state dipole

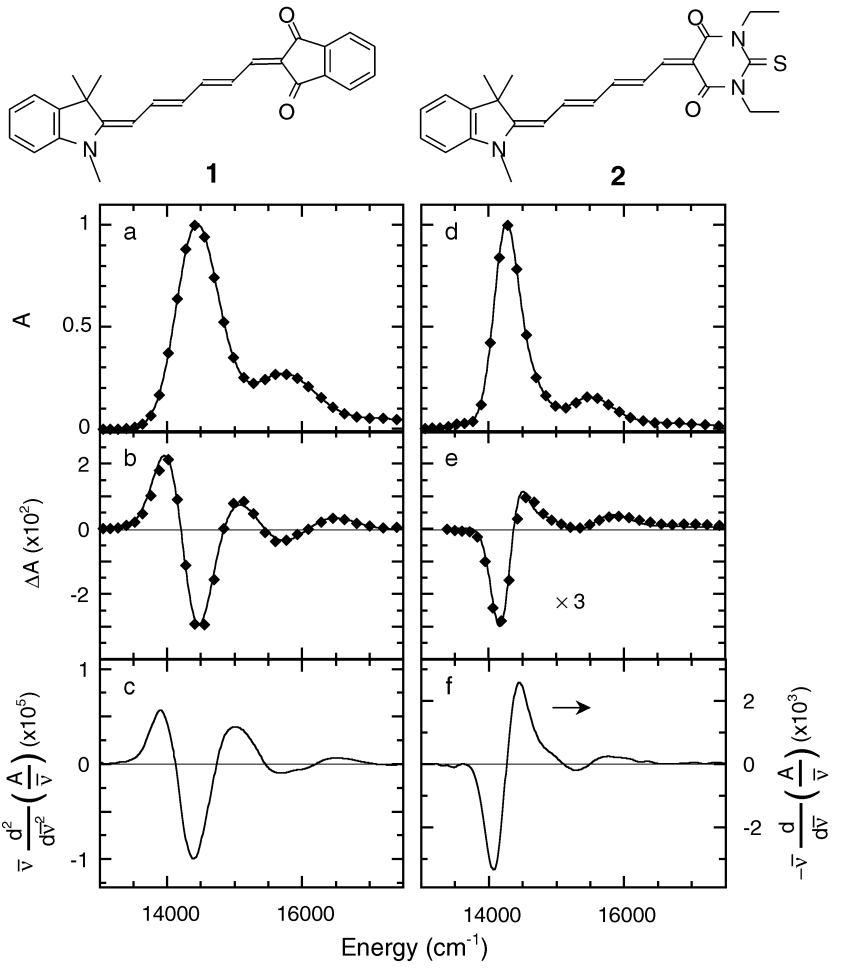

Figure 3 Stark spectra showing the acceptor dependence of the electronic structure in donor/acceptor polyenes. (*a*) Absorption spectrum, (*b*) ΔA (Stark) spectrum, and (*c*) $\bar{\nu}$-weighted second derivative of the absorption spectrum for **1** in frozen 2-MeTHF. Comparison of panels *b* and *c* demonstrates that the Stark effect is dominated by a second derivative contribution due to $\Delta\mu$. (*d*) Absorption spectrum, (*e*) ΔA (Stark) spectrum, and (*f*) negative $\bar{\nu}$-weighted first derivative of the absorption spectrum for **2** in frozen 2-MeTHF. Comparison of panels *e* and *f* (also cf panel *c*) shows that the Stark effect is dominated by a negative first derivative contribution because of a negative $\Delta\alpha$. For the absorption and ΔA spectra, both data (♦♦) and fit (—) are shown. All spectra were scaled to a peak absorbance of unity and a field strength of 1×10^6 V/cm to facilitate comparisons. The ΔA spectrum for **2** was multiplied by a factor of three to increase visibility of the data.

moments (and thus $\Delta\mu$) increased considerably. The structure of the connecting bridge in a donor/acceptor polyene, i.e. its position in between the limits outlined above, is thus only weakly affected by the length of the bridge, a result that agrees with theoretical predictions (38).

Variations in solvent polarity lead to an effect similar to that of variations of the donor and acceptor end groups on the bridge structure. A polar solvent environment preferentially stabilizes a ground state structure with more charge separation, i.e. a structure closer to limit **E**. In a nonpolar solvent the amount of such preferential stabilization is small, and the molecule will prefer a structure closer to limit **A**. The Stark spectra presented above for compounds **1** and **2** were taken in a solvent matrix of frozen 2-MeTHF. Figure 4 shows those spectra along with Stark spectra taken in frozen toluene and EtOH solutions. Both compounds show significant changes in their electro-optic response that are obvious even at a qualitative level and consistent with a significant shift of their structure toward limit **A** in toluene and toward limit **E** in EtOH (34).

Because molecular parameters may depend on solvent polarity and Stark spectra are obtained in frozen solvents, it is necessary to carefully consider the effect of freezing on the solvent polarity. Although no generally agreed upon definition of the term solvent polarity exists, it can be viewed in its broadest sense as the sum of interaction forces between solvent and solute (39). These forces are in competition with the thermal movement of the molecules. Upon freezing the solvent, the thermal motions are reduced drastically, and this will lead to a pronounced increase of the solvent polarity. This effect can be observed in the large spectral shifts upon freezing of solvent polarity indicators such as Reichardt's Dye[2] (39a) and also explains the differences in electronic structure found for the same molecule in liquid and frozen solution (34, 40).

Donor/acceptor polyenes have been proposed as a class of chromophores with enhanced second-order nonlinear optical properties (needed for applications such as frequency doubling of light and electro-optic switching). The commonly used two-level approximation predicts the molecular hyperpolarizability β (which is the figure of merit of a chromophore's second-order nonlinear response) to be proportional to the difference dipole moment between the ground and first excited state, i.e. $\beta \propto \Delta\mu$. This prediction has been explored using Stark spectroscopy (36, 37, 40) and has been shown to be in good quantitative agreement for moderately perturbed donor/acceptor polyenes where $\Delta\mu$ is large (37). Furthermore, the observed solvent dependence of β was shown to be correlated with similar changes in $\Delta\mu$, and for strongly perturbed polyene bridge structures, the observed decrease in β is accompanied by a decrease in $\Delta\mu$ (40).

Wortmann et al showed that different vibronic transitions concealed under the broad absorption band of 1,8-diphenyl-1,3,5,7-octatetraene are expected

[2] 2,6-diphenyl-4-(2,4,6-triphenylpyridino)phenolate.

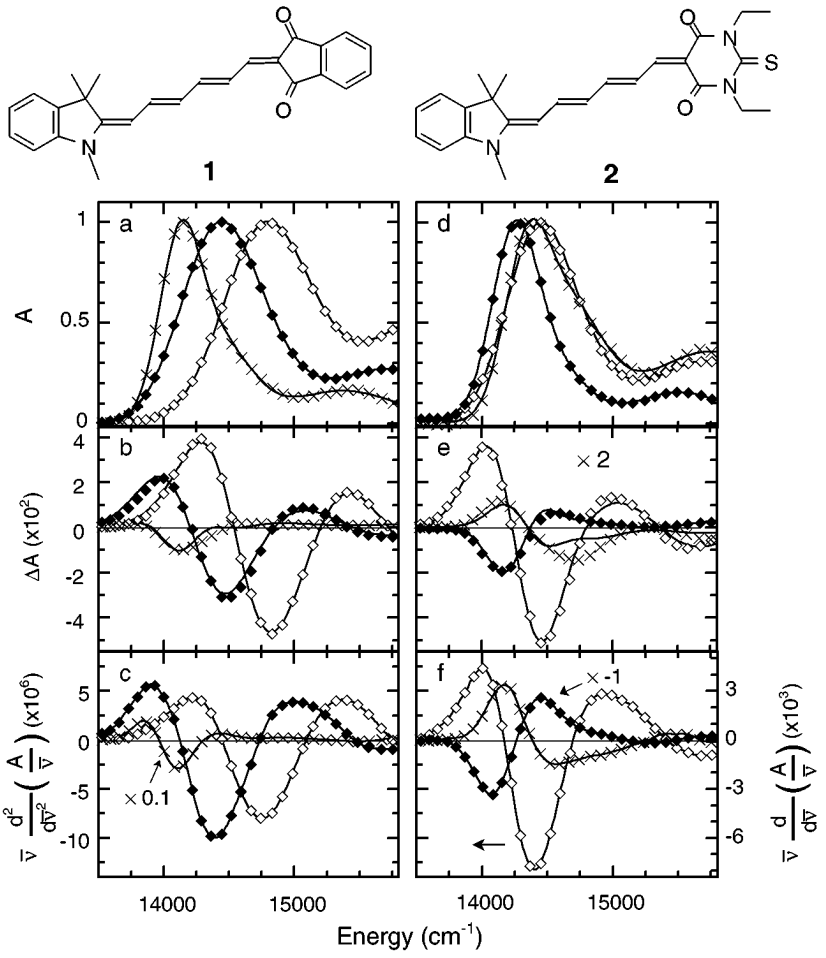

Figure 4 Use of the Stark effect to measure the solvent dependence of the electronic structure in donor/acceptor polyenes. (*a*, *d*) Absorption spectra, (*b*, *e*) ΔA (Stark) spectra, and (*c*, *f*) $\bar{\nu}$-weighted derivatives of the absorption spectra for **1** and **2**, respectively, in frozen EtOH, 2-MeTHF and toluene. For **1** and **2** (toluene) the second derivative is shown, for **2** (EtOH) the first derivative, and for **2** (2-MeTHF) the negative first derivative. For the absorption and ΔA spectra both data [(××, EtOH), (♦ ♦, 2-MeTHF), and (◇ ◇, toluene)] and fit (—) are shown. The derivatives are labeled using the same symbols. All spectra were scaled to a peak absorbance of unity and a field strength of 1×10^6 V/cm to facilitate comparisons. ΔA spectra for **2** were multiplied by a factor of two. The derivative for **1** (EtOH) was divided by a factor of ten to increase visibility of the other data. The differences in the molecule's electro-optic response are consistent with a molecular structure corresponding to a position between limits **A** and **B**, around **B**, and close to **C** for **1** and between limits **B** and **C**, close to **C**, and around **D** for **2** in toluene, 2-MeTHF, and EtOH, respectively.

to have very different electro-optic parameters (22). Values extracted from an electroabsorption spectrum thus will reflect an average value of these parameters. In cases where different vibronic bands can be distinguished in the absorption spectrum and the electro-optic response of the different bands can be deconvolved, the extracted values are expected to differ. Heterogeneity in the electro-optic response of different vibronic bands has been noted in a variety of donor/acceptor-substituted polyenes (34, 35, 41, 42). There is usually considerable overlap of the different vibronic bands, so it is difficult to extract meaningful values of $|\Delta\mu|$ for the different transitions. Higher-order Stark spectroscopy (HOSS) can be a useful tool in these cases, as shown in Figure 5, which compares the conventional (2ω) and higher-order (4ω) Stark spectra of compound **3**, a carotenoid derivative in which one end of a β-carotene molecule has been replaced with a very strong electron acceptor. The 2ω Stark effect for this molecule is huge (panel *b*, data indicated as ♦ ♦) and is dominated by a second derivative lineshape (cf panel *c*); however, a single set of fitting parameters (*dashed line*) cannot account for the molecule's electro-optic response. The absorption spectrum (panel *a*) clearly shows the presence of multiple vibronic bands, and a best fit using four sets of fitting parameters (with all four zeroth derivative components fixed at $A_\chi = 0$ to reduce the number of fitting parameters) gives good agreement between data and fit (*solid line*). The accuracy of the values of $|\Delta\mu|$ and $\Delta\alpha$ extracted from this fit, however, is questionable, since fits leading to very different values can give reasonable agreement with the data. In cases like this HOSS can provide additional data that can greatly constrain the values. If a Stark spectrum is dominated by $\Delta\mu$, i.e. the conventional Stark spectrum has a dominant second derivative lineshape, the 4ω Stark spectrum is expected to resemble the second derivative of the conventional (2ω) Stark spectrum. This is shown in the panels on the right side of Figure 5. The fourth-order Stark spectrum of compound **3** is shown along with the $\bar{\nu}$-weighted second derivative of the second-order Stark spectrum, scaled to match different regions of the fourth-order spectrum. From the scaling factor the value of $\underline{f} \cdot |\Delta\mu|$ can be deduced: 59 D below 12000 cm^{-1}, 42 D in the region between 12000 and 13500 cm^{-1}, and 35 D above 14000 cm^{-1}. The comparison of lineshapes insures that the Stark effect is dominated by $\Delta\mu$, and the weighted comparisons make it possible to extract meaningful information on the variation of $\Delta\mu$ for the different vibronic components.

Metal-to-Ligand, Ligand-to-Metal, and Metal-to-Metal Charge Transfer Transitions

The splitting of the degeneracy of the d-orbitals by the electric field of the ligands in coordination complexes is an example of a Stark splitting. In spite of this and the ubiquity of charge transfer (CT) transitions in transition metal complexes,

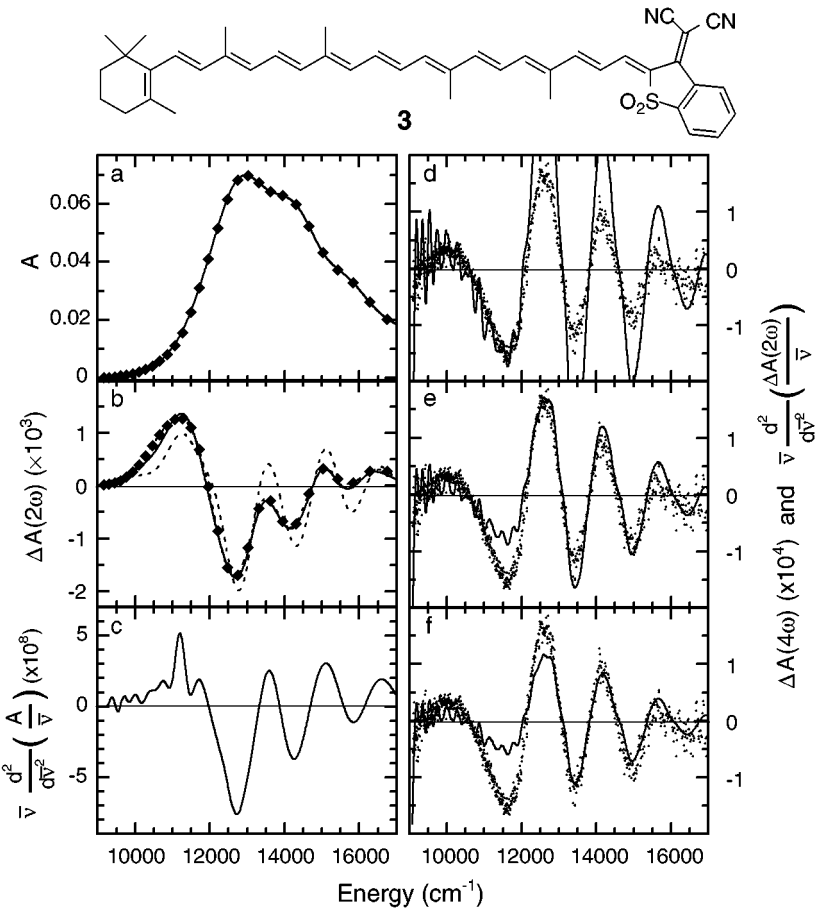

Figure 5 (*a*) Absorption spectrum, (*b*) conventional (i.e. second-order) Stark spectrum (applied external field 0.683 MV/cm), (*c*) $\bar{\nu}$-weighted second derivative of the absorption spectrum of **3** taken at 77 K in a frozen glass of 2-MeTHF. For the absorption and Stark spectra the data is represented by symbols (♦ ♦), and the result of the simultaneous best fit of the A and ΔA data is superimposed as a solid line. Two fits of the Stark spectrum are shown, using only one set of parameters (- - -) and four parameter sets with the zeroth derivative coefficients fixed at $A_\chi = 0$ (—) (see text). (*d*, *e*, and *f*) Fourth-order Stark spectrum ($\cdots$) and $\bar{\nu}$-weighted second derivative of the second-order Stark spectrum (—) of **3** taken at 77 K in a frozen glass of 2-MeTHF. Both spectra were scaled to a field strength of 1 MV/cm using F^4 and F^2 dependence, respectively (data was obtained with $A_{\max} = 0.065$, $F = 0.82$ MV/cm, external angle $\chi = 90^\circ$). The derivative of the second-order Stark spectrum was scaled to match different regions of the fourth-order spectrum. Scaling factors: (*d*) 35000, (*e*) 18000, (*f*) 12250, corresponding to $\underline{f} \cdot |\Delta\mu| = 59$ D, 42 D, 35 D, respectively. The scatter of the data points in the fourth-order spectrum is due to the statistical noise of the data and is similar to that for the conventional Stark spectrum (but note the difference in magnitude of the signals).

electroabsorption methods were not applied systematically to coordination compounds until Oh & Boxer reported the Stark spectra of metal-to-ligand CT (MLCT) transitions in mononuclear ruthenium complexes (43). For all the compounds studied, the amount of CT estimated from $|\Delta\mu|$ was significantly less than one would have expected from the distance between the metal and ligand. This deviation depends strongly on the nature of the ligand. For Ru(2,2′-bpy)$_3^{2+}$ (2,2′-bpy = 2,2′-bipyridine), the experimentally determined $|\Delta\mu|$ was equivalent to a transfer of one electron over a distance corresponding to (65/f)% of the metal-ligand separation (based on the distance from the metal to the geometric center of a bipyridine ligand). For Ru(NH$_3$)$_5$pz^{2+} (pz = pyrazine), this amounted to (32/f)%, while upon protonation of the ligand to Ru(NH$_3$)$_5$pzH^{3+}, no significant amount of CT was observed. No such effect of protonation was found for Ru(NH$_3$)$_5$(4,4′-bipyridine)$^{2+}$; on the contrary, in this case CT increased from (58/f)% to (73/f)%. Reimers & Hush (28, 44) suggested two main origins for this apparent lack of electron transfer: π back-bonding and effects of electrostatic interactions with spectator ligands. The latter was estimated to account for approximately half the difference for Ru(NH$_3$)$_5$L^{2+} compounds and is mainly due to interactions between the NH$_3$ dipoles and the metal charge. Back-bonding to ligand π^* orbitals delocalizes part of the metal charge to the ligand and thus leads to a partial transfer of charge in the ground state already.

Shin et al (45, 46) explored further variations in the Ru(NH$_3$)$_5$L^{2+} theme by measuring Stark spectra for compounds containing a variety of substituted pyridine ligands. Again, the experimentally determined electron transfer distances were smaller than the metal-ligand separation. Good agreement between expected CT distances and experimentally determined values could be reached by including two additional factors, π back-bonding and changes in the distribution of electrons in the ligand. Mixing of the localized states on metal and ligand (π back-bonding) was calculated using a two state model. Redistribution of charges in the ligand itself in response to the changed charge of the metal center was estimated using simple electrostatic arguments. The authors pointed out that in order to include interactions with the NH$_3$ spectator ligands, as suggested by Reimers & Hush, the change in polarizability $\Delta\alpha$ between ground and excited (CT) state has to be known accurately. Since, as discussed above, the magnitude of the A·$\Delta\mu$ cross terms in the first derivative component B$_\chi$ (Equation 3) is uncertain, the exact value of $\Delta\alpha$ is also unclear. While calculations based on a two-state model yield values for both the transition dipole moment ($\vec{m}$) and the difference in permanent dipole moment ($\Delta\mu$) that are in good agreement with experimental results, $\Delta\alpha$ cannot be estimated reliably this way and thus the influence of the spectator ligand is hard to estimate.

A somewhat related problem is the susceptibility of the CT transition to changes in the local electric fields present in its solvent environment. Oh &

Boxer (43) observed that for $Ru(NH_3)_5pz^{2+}$, similar Stark spectroscopic results were obtained in a frozen glycerol/water glass and a PVA polymer film (47), and these were also independent of the counterion (48). Shin et al (46) explored further whether changing the counterion or ionic strength had any influence on the observed electro-optic response. For $Ru(NH_3)_5(4\text{-}pyCONH_2)^{2+}$ $\underline{f} \cdot |\Delta\mu|$ was found to be independent of differences in counterions (BF_4^-, $C1^-$, SO_4^{2-}) and ionic strength of the solution (varied by changing the compound's concentration and addition of NaCl) within experimental error (10–20%). The results indicate that the CT process is not greatly affected by changes in its local electrostatic environment. This supports the conclusion that the interactions of the metal and ligand with the dipole moments of the NH_3 spectator ligands are negligible in this case.

Shin et al (45, 46) also studied what can be viewed as the reverse process, transfer of an electron from the ligand to the metal (LMCT transitions), in Ru(III) analogs of the same compounds [i.e. for $Ru(NH_3)_5L^{3+}$]. The observed effective electron transfer distances for these LMCT transitions were larger than the ones found for the MLCT transitions in the corresponding Ru(II) compounds. This difference is mainly due to decreased mixing of the localized states on metal and ligand (π bonding). Since the energy gap between the metal's t_{2g} orbital and the ligand's lowest unoccupied molecular orbital (LUMO) (π orbital) usually increases upon oxidation of the metal, the interaction between those orbitals will decrease and lead to less electron delocalization in the ground state. Overall the results for the LMCT transitions gave similar good agreement with calculated values after including corrections for π bonding and charge reorganization in the ligand, as discussed above.

Coupling between ligand and metal will not only affect transitions involving both (i.e. MLCT and LMCT transitions) but also those that formally involve only one of the two moieties, e.g. ligand-centered transitions. Hug & Boxer (49) studied the dipolar character of the ligand-centered transitions in a series of tris-2,2′-bipyridine complexes $M(2,2'\text{-}bpy)_3^{2+}$ with M = Zn, Fe, Os, Ru. The Stark spectrum of 2,2′-bipyridine has a dominant first derivative lineshape with only small second derivative contributions ($\underline{f} \cdot |\Delta\mu| = 0.5$ D). In the coordination compounds, however, the second derivative contributions to the lineshape were significant and dominated the Stark spectrum for M = Os and Ru ($\underline{f} \cdot |\Delta\mu| = 3.5$ D and 4.6 D, respectively). The extracted values of $|\Delta\mu|$ increased with decreasing energy separation between the MLCT and the ligand-centered transition, indicating coupling of the two transitions.

Oh & Boxer reported the first Stark spectroscopic determination of the extent of the metal-to-metal electron transfer process in mixed valence compounds (16); they studied $[(NH_3)_5Ru(II)\text{-}pz\text{-}Ru(III)(NH_3)_5]^{5+}$ (**4**) and $[(NH_3)_5Ru(II)$–4,4′-bpy–$Ru(III)(NH_3)_5]^{5+}$ (**5**).

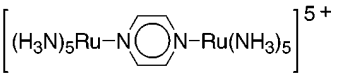

4

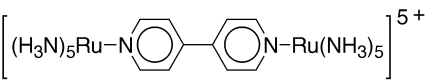

5

For the latter compound containing a 4,4′-bipyridine bridge, a large amount of CT transfer was found ($\underline{f} \cdot |\Delta\mu| = 28$ D), indicating that the ground state structure is localized with a reversal of the direction of the ground state dipole moment upon excitation of the mixed valence transition [i.e. Ru(II)–4,4′-bpy–Ru(III) → Ru(III)–4,4′-bpy–Ru(II)]. This corresponds to an effective electron transfer distance of (52/$\underline{f}$)% of the metal-metal seperation, and similar arguments, as outlined above for mononuclear Ru compounds, can be used to explain this deviation from transfer of a charge over the full metal-metal distance. In contrast, if the bridging ligand consists of a pyrazine molecule (the Creutz-Taube complex), no appreciable amount of CT upon excitation was observed, demonstrating the strong coupling between the Ru metal centers. In this case the ground state structure is best described as delocalized, and each Ru center has an effective charge of +2.5. Even at a qualitative level, these data provide clear information on the degree of localization in mixed valence systems.

In the mono-valence analogs of these compounds {i.e. $[(NH_3)_5$Ru(II)-pz-Ru(II)$(NH_3)_5]^{4+}$ and $[(NH_3)_5$Ru(II)–4,4′-bpy–Ru(II)$(NH_3)_5]^{4+}$}, MMCT transitions are not favored. However, now a MLCT transition can originate on one or the other Ru metal center. In the case of weak coupling between metal and ligand, a localized transition can be expected:

$$\text{Ru(II)-L-Ru(II)} \rightarrow \text{Ru(II)-L}^{-}\text{-Ru(III)} \qquad [\text{or} \rightarrow \text{Ru(III)-L}^{-}\text{-Ru(II)}],$$

and $\Delta\mu$ is expected to be large, leading to a second derivative lineshape of the ΔA spectrum. On the other hand, if the coupling between metal and ligand is large, the two transitions will also be strongly coupled and lead to a delocalized species:

$$\text{Ru(II)-L-Ru(II)} \rightarrow \text{Ru}\left(\text{II}\tfrac{1}{2}\right)\text{-L}^{-}\text{-Ru}\left(\text{II}\tfrac{1}{2}\right),$$

and no net change in dipole moment will occur. The ΔA spectrum in this case is expected to be dominated by the changes in polarizability upon excitation and should have a first derivative lineshape (28). The ΔA spectra of the two studied compounds are complicated, probably because of the presence of overlapping bands originating from different transitions, which prevents a quantitative analysis. However, in the wavelength region corresponding to the main absorption peak, the Stark spectrum is dominated by a first derivative lineshape

if L = pyrazine and by a second derivative lineshape if 4,4′-bipyridine is the bridging ligand. In the latter case the magnitude of the ΔA signal equals that of the ΔA signal observed for $Ru(NH_3)_5(4,4'\text{-bpy})^{2+}$, indicating a similar value of $\Delta\mu$.

Reimers & Hush (28) pointed out that the presence of two MLCT transitions that can be coupled with each other can lead to deviations from the simple sum-of-derivatives analysis as predicted by Equation 1. This will occur for an intermediate coupling strength, i.e. in between the two limits outlined above. In this case the change in dipole moment upon excitation becomes strongly dependent on the reaction coordinate δ, leading to different values of $\Delta\mu$ for transitions involving different vibronic levels (usually of the excited state). A similar heterogeneity of the electro-optic parameters concealed by one inhomogeneously broadened absorption band was also pointed out by Wortmann et al (22) for the case of a centrosymmetric polyene.

Karki et al (50) recently reported the electro-absorption spectrum of the MMCT transition in another system, $[(NC)_5Fe(II)\text{-}CN\text{-}Os(III)(NH_3)_5]^-$ (**6**). In this case the effective electron transfer distance corresponded to only (61/f)% of the metal-to-metal separation distance. This value was used to assess the solvent reorganization energy λ_s associated with the electron transfer process as well as the electronic coupling matrix element H_{ab} between the two metal sites. Both values are rather different from the ones derived using the assumption of electron transfer over the full metal-to-metal separation distance, i.e. λ_s is about two thirds smaller, while H_{ab} is about two times larger than previously expected.

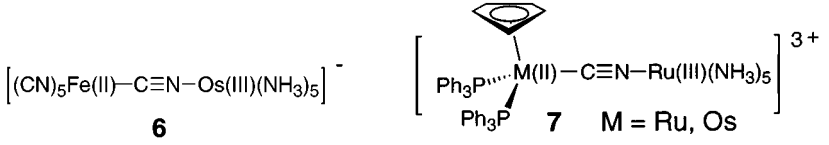

Preliminary results for $(PPh_3)_2cpRu(II)\text{-}CN\text{-}Ru(III)(NH_3)_5$ and $(PPh_3)_2cpOs(II)\text{-}CN\text{-}Ru(III)(NH_3)_5$ (**7**) yield very large $\Delta\mu$ values corresponding to about (90/f)% of the metal-to-metal separation distance. Thus the nature of the bridge is not the only variable that strongly affects the extent of the MMCT process.

TICT States

The dual fluorescence observed for various aromatic donor/acceptor systems is believed to result from the formation of a twisted intramolecular charge transfer (TICT) state. Whereas in the ground state the donor and acceptor groups are usually coplanar with large orbital overlap, the TICT state is characterized

by minimum orbital overlap and a large dipole moment. Rettig & Baumann (51) recently reviewed this field with an emphasis on the application of electro-optic methods in studies of such systems. Electric-field effect studies of the fluorescence of 2,6-N,N-tetramethyl-4-cyanoaniline in the gas phase revealed a large excited state dipole moment of about 12 D (52). Measurements on liquid solutions in different solvents yielded the same value after correction for the solvent-induced dipole moments. Sinha & Yates (53, 54) studied the electroabsorption of planar and conformationally twisted analogs of nitroaromatics and nitroanilines. While the planar systems showed only moderate values of $\Delta\mu$, the sterically hindered systems, in which the donor and acceptor groups are forced into an orthogonal conformation with respect to each other, showed large values of $\Delta\mu$.

Vibrational Stark Effects

Most vibrational Stark effect studies were limited to small molecules adsorbed on metal surfaces (55–57). Chattopadhyay & Boxer (18) demonstrated that the same methods used for electronic Stark spectroscopy can be extended into the infrared and reported the vibrational Stark effect (VSE) for the CN stretch ($\underline{f} \cdot |\Delta\mu| = 0.05$ D $\pm$ 0.02 D; $\zeta_A \approx 0^\circ$) of anisonitrile in a toluene glass. The measured value of $|\Delta\mu|$ can be converted to a Stark tuning rate of $(0.8 \pm 0.3) \times 10^{-6}$ cm^{-1} $\cdot$ (V/cm)$^{-1}$ if the electric field is applied along the CN bond direction. This represents the sensitivity of the vibrational frequency to an electric field and could be used to probe local electric fields in ordered systems such as proteins.

Inspired by this result, Hush and coworkers calculated the VSE at different levels of approximation (58, 59). The values obtained for the $\Delta\mu$ of the CN stretch for an isolated HCN or CH_3CN molecule were more than an order of magnitude smaller than the experimentally found value for anisonitrile in frozen toluene (18) or for CH_3CN in frozen 2-MeTHF (59a), and the gas-phase VSE spectrum was predicted to be dominated by a first derivative response, mainly due to cross terms between A_{ij} and $\Delta\mu$ (cf Equation 3). Much better agreement between calculation and experiment could be obtained by including the solvent in the calculations. Thus it may be that VSE spectroscopy will prove to be as powerful a tool for studying the interaction between solutes and solvents as it is for studying the properties (such as the anharmonicity) of individual vibrators.

Applications to Biological Systems

Many proteins contain functionally important prosthetic groups whose electronic absorption is in the visible or NIR region of the spectrum. This includes photosynthetic systems that have been extensively investigated by Stark spectroscopy and which are reviewed elsewhere (13, 32). Hole burning Stark

experiments on heme prosthetic groups have been carried out to obtain information on the distribution and origin of electric fields inside proteins and on the distribution and randomness of the protein structure (6, 60, 60a, 61).

Changes in the absorption and fluorescence of tryptophan in the near UV are widely used to characterize the local polarity within peptides and proteins. These spectral shifts are an internal Stark effect in which the intrinsic dipole moment change of the tryptophan chromophore interacts with the electrostatic field of the protein. In order to calibrate these shifts, information is needed on $\Delta\mu$. Pierce & Boxer have measured Stark spectra for two tryptophan derivatives and the peptide melittin that contains a single tryptophan residue (62). This experiment (and data on tryptophan in proteins) is complicated by the presence of two overlapping electronic transitions, labeled ^1L_a and ^1L_b, whose electro-optic response has to be separated in the analysis of the Stark spectra. In the case of tryptophan this separation is possible because the transition moments of the two states are nearly orthogonal, and all fluorescence has been found to originate from the ^1L_a state. The experimentally determined fluorescence anisotropy can thus be used to deconvolve the absorption spectra of the two states. From a simultaneous fit of the absorption, Stark, and fluorescence anisotropy spectra, $\underline{f} \cdot |\Delta\mu|$ was found to be about 6.0 D for the ^1L_a state in melittin and *N*-acetyl-*L*-tryptophanamide, a value that is larger than estimated by calculations. The angle ζ_A between the transition moment and $\Delta\mu$ is between 60° and 80° in both cases. For the other derivative, 5-methoxytryptophan, the absorption spectra of the two states are shifted in such a way that the ^1L_a state is fully concealed by the ^1L_b state. A decomposition of the two absorption bands and thus of the Stark response of the two states was not possible in this case.

Chattoraj et al (63) recently reported the Stark spectrum and photophysics of the green fluorescent protein (GFP). This protein is remarkable in that its chromophore is not exogenously supplied but forms autocatalytically in a cyclization reaction of three amino acid residues. The environment of the chromophore plays an essential part in this intense fluorescence, as unfolding of the protein results in total loss of the fluorescence. The Stark spectroscopic results (63) for the excitation process ($\underline{f} \cdot |\Delta\mu| = 6.8 \pm 0.3$ D with $\zeta_A = 21 \pm 7°$) can yield valuable information on the nature of this excited state. Other remarkable features of this protein are the dramatic spectral changes of its fluorescent properties upon point mutations in either the amino acids forming the chromophore or in others located in the chromophore's environment in the folded protein. A comparative Stark spectroscopic study of wild-type GFP and two such mutants is under way.

Other Applications

In the following, we collect results from diverse fields where Stark spectroscopy has been used. In many cases the analysis of the spectra was not carried out

in the context of Equation 1, either because the focus was more on qualitative aspects or because additional factors that are not covered by the assumptions underlying Equation 1 had to be considered.

Langmuir-Blodgett (LB) film structures have been used to orient a number of different chromophores. In this case the linear and quadratic Stark effect can be observed directly, and this has been used to extract information on the electro-optic parameters of the probe molecule (64, 65). A serious limitation of these experiments is the lack of information on the degree of orientation that can be achieved in the LB film. Hole burning Stark experiments have shown that a considerable distribution in the orientation of a probe molecule with respect to the externally applied field can exist (66, 67). The electro-optic response of a probe molecule has also been used to study the electric field present within as well as across a membrane structure (68–70). So-called voltage-sensitive dyes (71) are widely used to probe the transmembrane potential that is especially important in membranes associated with the nervous system. By using a sharp cut-off filter such that the dye fluorescence is either passed or rejected in an epi-fluorescence microscope, sensitive local information on membrane potential variations can be obtained.

Many crystalline organic materials exhibit photoconductivity, that is, charge carriers are generated when the crystals are irradiated. These effects are of widespread interest in the photography, photocopier, and detector industries. In order to obtain a deeper understanding of the mechanism of carrier generation, Sebastian et al (72, 73) studied the electroabsorption spectra of crystalline polyacenes (anthracene, tetracene, pentacene) and observed ΔA spectra with dominant second derivative lineshapes, which they attributed to the presence of CT transitions between neighboring molecules in the crystal. This interpretation of the spectra, however, has been challenged, and the lineshapes were alternatively attributed to the presence of a set of degenerate CT states that possess no net dipole moment (30).

Electric-field effects on both the absorption and reflectance spectra of conjugated polymers have been studied extensively (74–80). These materials are of great interest for potential applications in nonlinear optics, and their electroabsorption spectra can be related to their third-order nonlinear response $\chi^{(3)}$ through a Kramers-Krönig relationship (81, 82). The magnitude of the ΔA signal was found to be strongly dependent on the relative orientation of the field. If it is aligned parallel to the polymer chain, the electro-optic response is very large and the electronic structure of the conjugated polymer resembles the band structure of a semiconductor (74–76). The lineshapes of the ΔA spectra in these systems were also found to be dependent on the texture of the sample. While crystalline polydiacetylene samples exhibit a dominant first derivative lineshape, Soos et al (80) found film samples with large second

derivative contributions, which were attributed to interactions of closely spaced transitions. A similar texture dependence of the ΔA signal was proposed for the electro-absorption spectra of polyacenes (83).

The presence of an electric field can activate mixing of different states within a molecule. Effects of this kind are not covered by the assumptions underlying Equation 1 and will lead to additional features in the ΔA spectrum. For example, in the electroabsorption spectrum of poly(di-n-hexylsilane) a large feature can be observed at an energy corresponding to a two-photon–allowed state (84). The electroabsorption spectrum of C_{60} was interpreted in terms of electric-field–induced splitting and mixing of molecular energy levels (85), but the data were also described as indicative for the presence of CT states (86). For both C_{60} and C_{70}, the electroabsorption signal has been used to establish the nature of the dominant channel for third-order nonlinear optical processes (87).

While Equation 1 rests on the assumption of a transition to an isolated state, the electronic structure of solid state materials like semiconductors is very different. Electric-field effects have often been employed to study the electronic band structure of these materials (88, 89). Electroabsorption spectroscopy has also been used in studies of quantum-confined systems, such as GaAs/AlGaAs quantum wells (90). Another area on which much attention has been focused recently are semiconductor microcrystallites, small semiconductor particles at the border between atomic/molecular and bulk behavior, whose Stark spectra are not well understood (91). The dominant second derivative lineshape observed for randomly oriented CdSe microcrystallites has been interpreted as evidence for the presence of dipolar excited states in these otherwise very symmetric systems (92). This interpretation, however, has been challenged, and the observed spectra were interpreted to be due to the activation of dark states by the presence of the external electric field (31).

Finally, electric-field effect spectra of single molecules have been reported in recent years (93, 94). This approach lifts one of the limitations of conventional Stark and hole burning Stark spectroscopy in which the simultaneous response of many molecules is observed and thus only averaged information is obtained. For terylene molecules in a polyethylene matrix, measured at low field strengths (up to 1.5 $kV \cdot cm^{-1}$), Orrit et al (94) observed linear shifts in electric-field strength. This linear Stark effect is associated with the presence of matrix-induced dipole moments that were found to vary from molecule to molecule, revealing differences in the local electrostatic field present at different sites that the probe molecules occupy in the guest matrix. For pentacene embedded in a *p*-terphenyl crystal, the shifts were quadratic in field strength (measured at higher field strengths of up to 30 $kV \cdot cm^{-1}$) (93). This dominance of the quadratic Stark effect demonstrates that the internal field of the *p*-terphenyl guest crystal is rather small.

ACKNOWLEDGMENTS

Work done in our laboratory over the past 10 years and reported in this review has been sponsored by the NSF Chemistry Division (coordination compounds, vibrational Stark effects, donor/acceptor polyenes), the NSF Biophysics Program (photosynthetic systems), the National Institutes of Health (tryptophan) and the ONR (GFP) under Contract N00014-91-C-0170 to the Stanford FEL Center. SGB wishes to thank Professor Noel Hush for many stimulating discussions and suggestions.

Literature Cited

1. Hanson DM, Patel JS, Winkler IC, Morrobel-Sosa A. 1983. In *Spectroscopy and Excitation Dynamics of Condensed Molecular Systems*, ed. VM Agranovich, RM Hochstrasser. *Modern Problems in Condensed Matter Sciences*, Ser. ed. VM Agranovich, AA Maradudin, 4:621–79. Amsterdam: North-Holland
2. Hochstrasser RM. 1973. *Acc. Chem. Res.* 6:263–69
3. Meixner AJ, Renn A, Bucher SE, Wild UP. 1986. *J. Phys. Chem.* 90:6777–85
4. Moerner WE, ed. 1988. *Persistent Spectral Holeburning: Science and Applications*. Berlin: Springer-Verlag
5. Kohler BE, Woehl JC. 1995. *J. Chem. Phys.* 102:7773–81
6. Gafert J, Friedrich J, Vanderkooi JM, Fidy J. 1995. *J. Phys. Chem.* 99:5223–27
7. Bogner U. 1996. In *Molecular Electronics: Properties, Dynamics and Applications*, ed. G Mahler, V May, M Schreiber, pp. 233–55. New York: Marcel Dekker
8. Liptay W. 1969. *Angew. Chem. Int. Ed. Engl.* 8:177–88
9. Liptay W. 1974. In *Excited States*, ed. EC Lim, 1:129–229. New York: Academic
10. Labhart H. 1967. In *Advances in Chemical Physics*, ed. I Prigogine, 13:179–204. London: Interscience
11. Baumann W. 1989. In *Physical Methods of Chemistry*, ed. BW Rossiter, JF Hamilton, 3B:45–131. New York: Wiley. 2nd ed.
12. Lao K, Moore LJ, Zhou H, Boxer SG. 1995. *J. Phys. Chem.* 99:496–500
13. Boxer SG. 1993. In *The Photosynthetic Reaction Center*, ed. J Deisenhofer, JR Norris, 2:179–220. San Diego: Academic
14. Lockhart DJ, Hammes SL, Franzen S, Boxer SG. 1991. *J. Phys. Chem.* 95:2217–26
15. Lao K, Franzen S, Steffen M, Lambright D, Stanley R, Boxer SG. 1995. *Chem. Phys.* 197:259–75
16. Oh DH, Boxer SG. 1990. *J. Am. Chem. Soc.* 112:8161–62
17. Stocker JW, Hug S, Boxer SG. 1993. *Biochim. Biophys. Acta* 1144:325–30
18. Chattopadhyay A, Boxer SG. 1995. *J. Am. Chem. Soc.* 117:1449–50
19. Böttcher CJF. 1973. *Theory of Electric Polarization*, Vol. 1. Amsterdam: Elsevier. 2nd ed.
20. Franzen S, Boxer SG. 1993. *J. Phys. Chem.* 97:6304–18
21. Middendorf TR, Mazzola LT, Lao K, Steffen M, Boxer SG. 1993. *Biochim. Biophys. Acta* 1143:223–34
22. Wortmann R, Elich K, Liptay W. 1988. *Chem. Phys.* 124:395–409
23. Kador L, Jahn S, Haarer D, Silbey R. 1990. *Phys. Rev. B* 41:12215–26
24. Hartmannsgruber N, Maier M. 1992. *J. Chem. Phys.* 96:7279–86
25. Altmann RB, Renge I, Kador L, Haarer D. 1992. *J. Chem. Phys.* 97:5316–22
26. Vauthey E, Voss J, de Caro C, Renn A, Wild UP. 1994. *Chem. Phys.* 184:347–56
27. Altmann RB, Kador L, Haarer D. 1996. *Chem. Phys.* 202:167–74

27a. Moore LJ, Bublitz GU, Boxer SG. Unpublished results

28. Reimers JR, Hush NS. 1991. In *Mixed Valency Systems: Applications in Chemistry, Physics and Biology*, ed. K Prassides, pp. 29–50. Dordrecht: Kluwer Acad.
29. Talanina IB, Collins MA, Dubicki L, Krausz E. 1992. *Chem. Phys. Lett.* 200:318–24

30. Petelenz P. 1993. *Chem. Phys.* 171:397–405
31. Sacra A, Norris J, Murray CB, Bawendi MG. 1995. *J. Chem. Phys.* 103:5236–45
32. Boxer SG. 1996. In *Biophysical Techniques in Photosynthesis*, ed. J Amesz, AJ Hoff, pp. 177–89. Dordrecht: Kluwer Acad.
33. Liptay W, Wortmann R, Böhm R, Detzer N. 1988. *Chem. Phys.* 120:439–48
34. Bublitz GU, Ortiz R, Marder SR, Boxer SG. 1997. *J. Am. Chem. Soc.* 119:3365–76
35. Baumann W. 1983. *Z. Naturforsch. Teil A* 38:995–1002
36. Blanchard-Desce M, Wortmann R, Lebus S, Lehn J-M, Krämer P. 1995. *Chem. Phys. Lett.* 243:526–32
37. Blanchard-Desce M, Alain V, Midrier L, Wortmann R, Lebus S, et al. 1997. *J. Photochem. Photobiol. A.* In press
38. Gorman CB, Marder SR. 1995. *Chem. Mater.* 7:215–20
39. Reichardt C. 1988. *Solvents and Solvent Effects in Organic Chemistry.* Weinheim: VCH. 2nd ed.
39a. Bublitz GU, Boxer SG. 1997. *J. Am. Chem. Soc.* Submitted
40. Bublitz GU, Ortiz R, Runser C, Fort A, Barzoukas M, et al. 1997. *J. Am. Chem. Soc.* 119:2311–12
41. Gottfried DS, Steffen MA, Boxer SG. 1991. *Biochim. Biophys. Acta* 1059:76–90
42. Krawczyk S, Daniluk A. 1995. *Chem. Phys. Lett.* 236:431–37
43. Oh D, Boxer SG. 1989. *J. Am. Chem. Soc.* 111:1130–31
44. Reimers JR, Hush NS. 1991. *J. Phys. Chem.* 95:9773–81
45. Shin YGK, Brunschwig BS, Creutz C, Sutin N. 1995. *J. Am. Chem. Soc.* 117:8668–69
46. Shin YK, Brunschwig BS, Creutz C, Sutin N. 1996. *J. Phys. Chem.* 100:8157–69
47. Oh DH, Sano M, Boxer SG. 1991. *J. Am. Chem. Soc.* 113:6880–90
48. Oh DH. 1991. *Electric field (Stark) effects in inorganic and bioinorganic charge transfer complexes.* PhD thesis. Stanford Univ.
49. Hug SJ, Boxer SG. 1996. *Inorg. Chim. Acta* 242:323–27
50. Karki L, Lu HP, Hupp JT. 1996. *J. Phys. Chem.* 100:15637–39
51. Rettig W, Baumann W. 1992. In *Progress in Photochemistry and Photophysics*, ed. JF Rabek, 6:79–134. Boca Raton: CRC
52. Bischof H, Baumann W, Detzer N, Rotkiewicz K. 1985. *Chem. Phys. Lett.* 116:180–85
53. Sinha HK, Yates K. 1990. *J. Phys. Chem.* 93:7085–93
54. Sinha HK, Yates K. 1991. *Can. J. Chem.* 69:550–57
55. Bagus PS, Nelin CJ, Müller W, Philpott MR, Seki H. 1987. *Phys. Rev. Lett.* 58: 559–62
56. Lambert DK. 1988. *J. Chem. Phys.* 89: 3847–60
57. Lambert DK. 1996. *Electrochim. Acta* 41: 623–30
58. Hush NS, Reimers JR. 1995. *J. Phys. Chem.* 99:15798–805
59. Reimers JR, Zeng J, Hush NS. 1996. *J. Phys. Chem.* 100:1498–504
59a. Chattopadhyay A, Boxer SG. Unpublished results
60. Gafert J, Friedrich J, Parak F. 1995. *Proc. Natl. Acad. Sci. USA* 92:2116–20
60a. Fritsch K, Friedrich J, Parak F, Skinner JL. 1996. *Proc. Natl. Acad. Sci. USA* 93:15141–45
61. Geissinger P, Kohler BE, Woehl JC. 1995. *J. Phys. Chem.* 99:16527–29
62. Pierce DW, Boxer SG. 1995. *Biophys. J.* 68:1583–91
63. Chattoraj M, King BA, Bublitz GU, Boxer SG. 1996. *Proc. Natl. Acad. Sci. USA* 93:8362–67
64. Grewer G, Lösche M. 1991. *Makromol. Chem. Macromol. Symp.* 46:79–87
65. Ohta N, Ogata Y, Okazaki S, Yamazaki I. 1995. *Chem. Phys. Lett.* 244:355–62
66. Orrit M, Bernard J, Mouhsen A, Talon H, Möbius D, Personov RI. 1991. *Chem. Phys. Lett.* 179:232–36
67. Bernard J, Talon H, Orrit M, Möbius D, Personov RI. 1992. *Thin Solid Films* 217:178–86
68. Blinov LM, Palto SP, Yudin SG. 1989. *J. Mol. Electron.* 5:45–51
69. Palto SP, Barnik MI, Khavrichev VA, Davydova NN, Yudin SG. 1992. *Thin Solid Films* 217:167–73
70. Paschenko VZ, Vershinin AO, Churin AA. 1993. *J. Photochem. Photobiol. B* 18:127–30
71. Haugland RP. 1996. *Handbook of Fluorescent Probes and Research Chemicals.* Eugene, OR: Mol. Probes. 6th ed.
72. Sebastian L, Weiser G, Bässler H. 1981. *Chem. Phys.* 61:125–35
73. Sebastian L, Weiser G, Peter G, Bässler H. 1983. *Chem. Phys.* 75:103–14
74. Sebastian L, Weiser G. 1979. *Chem. Phys. Lett.* 64:396–400
75. Sebastian L, Weiser G. 1981. *Phys. Rev. Lett.* 46:1156–59
76. Sebastian L, Weiser G. 1981. *Chem. Phys.* 62:447–57

77. Phillips SD, Worland R, Yu G, Hagler T, Freedman R, et al. 1989. *Phys. Rev. B* 40:9751–59
78. Weiser G. 1992. *Phys. Rev. B* 45:14076–85
79. Mukhopadhyay D, Soos ZG. 1995. *J. Chem. Phys.* 104:1600–10
80. Soos ZG, Mukhopadhyay D, Hennessy MH. 1996. *Chem. Phys.* 210:249–57
81. Hutchings DC, Sheik-Bahae M, Hagan DJ, Van Stryland EW. 1992. *Opt. Quantum Electron.* 24:1–30
82. Rohlfing F, Bradley DDC, Eberhardt A, Müllen K, Cornil J, et al. 1996. *Synth. Met.* 76:35–38
83. Slawik M, Petelenz P. 1992. *Chem. Phys.* 167:377–84
84. Tachibana H, Kawabata Y, Koshihara S, Tokura Y. 1990. *Solid State Comm.* 75:5–9
85. Jeglinski S, Vardeny ZV, Moses D, Srdanov VI, Wudl F. 1992. *Synth. Met.* 49/50:557–63
86. Petelenz P, Slawik M, Pac B. 1994. *Synth. Met.* 64:335–39
87. Hess BC, Bowersox DV, Mardirosian SH, Unterberger LD. 1996. *Chem. Phys. Lett.* 248:141–46
88. Aspnes DE. 1980. In *Optical Properties of Solids*, ed. M Balkanski, *Handbook on Semiconductors*, Ser. ed. TS Moss, 2:109–54. Amsterdam: North-Holland
89. Pollak FH. 1994. In *Optical Properties of Semiconductors*, ed. M Balkanski, *Handbook on Semiconductors*, Ser. ed. TS Moss, 2:527–635. Amsterdam: Elsevier. Revised ed.
90. Miller DAB, Chemla DS, Damen TC, Gossard AC, Wiegmann W, et al. 1985. *Phys. Rev. B* 32:1043–60
91. Brus L. 1991. *Appl. Phys. A* 53:465–74
92. Colvin VL, Alivisatos AP. 1992. *J. Chem. Phys.* 97:730–33
93. Wild UP, Güttler F, Pirotta M, Renn A. 1992. *Chem. Phys. Lett.* 193:451–55
94. Orrit M, Bernard J, Zumbusch A, Personov RI. 1992. *Chem. Phys. Lett.* 196:595–600